ACS Medicinal Chemistry Letters

Letter

Cite This: ACS Med. Chem. Lett. 2018, 9, 452−456

Radiosynthesis and Evaluation of [^{11}C]HD-800, a High Affinity Brain Penetrant PET Tracer for Imaging Microtubules

Kiran Kumar Solingapuram Sai,[†,⊥] Jaya Prabhakaran,[‡,§] Gayathri Ramanathan,[†] Stephanie Rideout,[†] Christopher Whitlow,[†] Akiva Mintz,[∥] J. John Mann,[‡,§,∥] and J. S. Dileep Kumar*[,‡,⊥]

[†]Department of Radiology, Wake Forest School of Medicine, Winston Salem, North Carolina, United States

[‡]Molecular Imaging and Neuropathology Division, New York State Psychiatric Institute, New York, United States

[§]Department of Psychiatry, Columbia University Medical Center, New York, United States

[∥]Department of Radiology, Columbia University Medical Center, New York, United States

Supporting Information

ABSTRACT: Microtubules (MTs) are highly abundant throughout the cytoskeleton, and their dysfunction is implicated in the pathogenesis of malignancies, various neurodegenerative disorders, and brain injuries. Validated radiotracers reported so far for MTs are [^{11}C]paclitaxel, [^{18}F]fluoropaclitaxel, and [^{11}C]docetaxel; however, they are well-characterized substrates of efflux transporters and consequently have poor uptake into the brain due to minimal blood brain barrier (BBB) penetration. PET imaging of MT expression requires radiolabeled BBB penetrating MT ligands, and it may offer a direct and more sensitive approach for early diagnosis, monitoring disease progression, and treatment effects in brain diseases and assessing the clinical potential of targeted therapeutics and treatments. We have identified N-(4-methoxyphenyl)-N-5-dimethylfuro[2,3-*d*]pyrimidin-4-amine (HD-800) as a high affinity and selective colchicine site tubuline inhibitor amenable to radiolabel with C-11, a positron emitting isotope. HD-800 and desmethyl-HD-800 were synthesized in one step with 75% and 80% yields respectively from commercial synthons. The radiosynthesis of [^{11}C]HD-800 was achieved in 45 ± 5% yield at EOS. *Ex vivo* biodistribution binding data of [^{11}C]HD-800 indicate that the radioligand penetrated the BBB and it was retained in brain with 75% specific binding. Apart from the brain, specific binding was observed in muscle (55%), heart (50%), lungs (43%), blood (37%), and pancreas (30%). MicroPET imaging in mice showed excellent binding in brain that was blocked by preadministration of unlabeled HD-800 and a colchicine site binding MT ligand MPC-6827. The above results indicate that [^{11}C]HD-800 may be a suitable PET ligand for the *in vivo* quantification of MT inside and outside the brain.

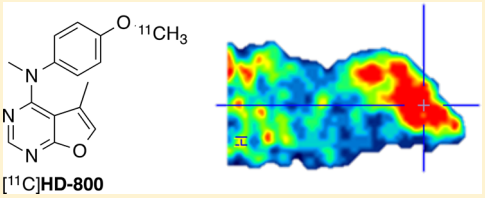

KEYWORDS: *Microtubule, brain, radiotracer, cytoskeleton*

Microtubules (MTs) are one of the cytoskeletal components that act as scaffolding or molecular shuttles for transporting vesicles, granules, organelles such as mitochondria, and chromosomes in cells.[1−3] MTs are highly abundant in mammalian brain and are present in approximately 20% of the total brain protein as compared with 3%−4% outside the brain.[4] Disruption of the structural integrity of the MT network and impairment of MT function are considered to be part of the pathophysiology of many central nervous system (CNS) disorders. Accordingly, stabilization of MT disruption or dynamics has emerged as a possible therapeutic approach for treating some CNS disorders.[5−9] MTs, specifically βIII-tubulin isoform is variously expressed in all types and grades of human gliomas, and its expression is significantly increased in high-grade gliomas, particularly in glioblastoma multiforme (GBM).[10,11] Therefore, βIII-tubulin may be a biomarker to distinguish high-grade and low-grade gliomas. Several BBB penetrating and non drug resistant microtubule targeting agents (MTAs) currently have been tested in clinical trials for GBM and other brain malignancies (e.g., synthetic and natural epothilones and TPI-288).[12−14] MT loss or reduction in MT mass in axons and dendrites is associated with aging and neurodegenerative and neuropsychiatric diseases.[5−7] Other diseases with MT pathophysiology in CNS include tauopathies in which tau a microtubule associated protein (MAP) protein dissociates from MT as a result of hyper-phosphorylation. The proof-of-principle experiments in animal models expressing human mutant tau suggest that BBB penetrant MTAs are potential treatments for Alzheimer's disease (AD) and other tauopathies. Two such agents BMS-241027 and TPI-288 have been tested in clinical trials in AD, progressive supranuclear palsy (PSP) and corticobasal degeneration (CBD).[15−17] Similar to AD, MT loss is reported in Parkinson's disease (PD), amyotrophic lateral sclerosis (ALS), hereditary spastic paraplegia (HSP), multiple sclerosis (MS), Huntington's disease (HD),[18−22] traumatic brain injury (TBI), chronic traumatic encephalopathy (CTE), and spinal cord injury (SCI).[23−25] Prominent changes in MT expression levels are also found in

Received: February 7, 2018
Accepted: April 30, 2018
Published: April 30, 2018

DOI: 10.1021/acsmedchemlett.8b00060
ACS Med. Chem. Lett. 2018, 9, 452−456

disease specific regions such as the hippocampus and prefrontal cortex in schizophrenia, major depressive disorder (MDD), and bipolar disorder (BPD).[26,27]

Therapeutic failures of older MTAs in brain disorders including malignancies have been attributed to the inability of drugs to cross the BBB due to their affinity for P-glycoprotein 1 (P-gp) and multidrug resistance protein 1 (MDR1) and the toxic effect in noncancerous cells. However, new generation MTA ligands circumvent these disadvantages and show promise in the treatment of brain malignancies.[12−14] Collectively, the reported results are exciting because they demonstrate that prevention/reversal of MT loss associated with neurodegeneration and brain injury can be therapeutic. Despite this, the lack of a valid MT based biomarker or imaging agent hampers drug development of MTAs for CNS disorders.

A BBB penetrating PET ligand that can quantify MT noninvasively would permit imaging a variety of CNS disorders and brain malignancies and enable the conduct of target occupancy screens of potential therapeutic drugs. However, most efforts in past decades were unsuccessful for the development of a BBB permeable PET ligand for MT. We recently reported [^{11}C]MPC-6827, a colchicine binding MT ligand as the first brain penetrant PET ligand that exhibits specific binding in rodent brain.[28] As a part of the development of specific PET ligands for MTs, we have identified N-(4-methoxyphenyl)-N-5-dimethylfuro[2,3-*d*]pyrimidin-4-amine (HD-800), a high affinity and selective colchicine site tubuline inhibitor (MT IC_{50} = 4.3 nM in the inhibition of the proliferation of MDA-MB-435 cells and EC_{50} 24 nM for MT depolymerization in A-10 cells) amenable for radiolabeling with [C-11].[29] HD-800 also exhibits high potency in inhibiting the growth of 47 cell lines from a NCI-60 cells panel (GI_{50} < 10 nM) and circumvents Pgp and βIII-tubulin mediated resistance in SK-OV-3 MDR1-M6/6 and HeLa WTβIII cells.[29] Furthermore, HD-800 shows higher tumor growth inhibition (TGI) than paclitaxel and also antidrug resistant properties in a variety of tumor xenografts.[36] Herein, we describe the radiosynthesis, *ex vivo* and *in vivo* evaluation of [^{11}C]HD-800 as a PET radiotracer for MT imaging in brain.

The synthesis of reference standard HD-800 was achieved via a reported procedure.[29] Since the yield of HD-800 (**3**) obtained was low (22%) from the reported procedure, we synthesized it via an alternative one step procedure which resulted in 77% yield by coupling commercial 4-chloro-5-methylfuro[2,3-*d*]-pyrimidine (**1**) with 4-methoxy-*N*-methylaniline (**2**) using diisopropyl ethylamine as the base (Scheme 1). HD-800 did not exhibit significant affinity to a variety of competitive brain receptors, transporters, biogenic amines, and proteins (K_i > 10 μM) based on National Institute of Mental Health−Psycho-active Drug Screening Program (NIMH-PDSP) binding assays. Desmethyl-HD-800 (**4**), the radiolabeling precursor was synthesized via the demethylation of compound **3** using BBr_3 in 85% isolated yield (Scheme 1). Alternatively, compound **4** was synthesized via the coupling of **2** with 4-(methylamino)-phenol (**5**) in 80% yield (Scheme 1). Radiosynthesis of [^{11}C]HD-800 was performed by reacting desmethyl precursor **4** with [^{11}C]CH_3I in a GE-FX2MeI/FX2M module in 45 ± 5% (n = 20) radiochemical yield (RCY) based on [^{11}C]CH_3I and with a molar activity of 92.5 ± 18.5 GBq/μmol at the end of synthesis (EOS) (Scheme 1). [^{11}C]HD-800 was stable in 5% ethanol-saline formulation under sterile conditions for 4 h (n = 4), and the $logP_{oct/wat}$ was estimated as 3.1 by a shake flask method.[30]

Scheme 1. Synthesis of HD-800 and Radiosynthesis of [^{11}C]HD-800

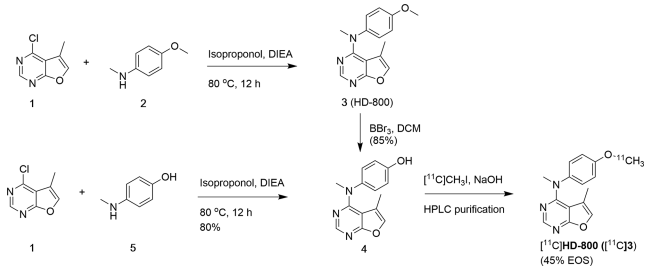

After the successful synthesis and reliable automation, we performed *ex vivo* biodistribution studies of [^{11}C]HD-800 in male white mice (n = 4) at 5, 30, and 60 min via tail vein administration. Our experiment shows that [^{11}C]HD-800 penetrated the BBB and retained in the brain (brain %ID/g = 5 ± 0.5% at 30 min), followed by a pronounced washout at 60 min (brain %ID/g = 1.5 ± 0.84%) (Figure 1). Blood, heart, lungs, spleen, pancreas, and muscles also show uptake of [^{11}C]HD-800. Liver and kidney exhibited high uptake of the radiotracer. We performed blocking experiments and measured the effect after 30 min of radiotracer injection based on the peak activity of [^{11}C]HD-800 in brain (Figure 1).

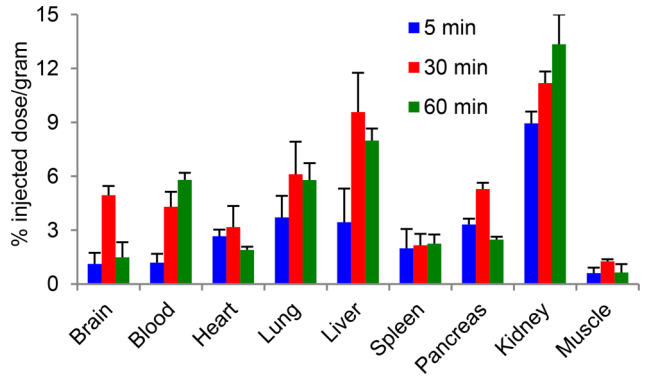

Figure 1. Baseline biodistribution of [^{11}C]HD-800 in male white mice (n = 4). Values are reported as the mean ± SD from four independent experiments.

Blocking experiments with unlabeled HD-800 (5 mg/kg, i.v) (n = 4) showed that after 30 min postinjection, 75% of the total binding of [^{11}C]HD-800 binding in brain was specific (Figure 2). In addition to brain, [^{11}C]HD-800 also exhibits specific binding in blood (36%), heart (50%), lungs (43%), pancreas (30%), and muscles (55%). Spleen, kidney, and liver did not show significant specific binding of [^{11}C]HD-800. Similar to brain, we have also noticed a relative slow washout of activity in heart, lung, liver, pancreas, and muscles. Based on the blocking experiments, the binding ratio of [^{11}C]HD-800 in brain was 4.5 times higher than in the muscle at 30 min.

Subsequently, we examined the *in vivo* brain imaging of [^{11}C]HD-800 in male white mice (n = 3) using the Trifoil Triumph II PET/CT scanner for a 60 min acquisition (Figure 3). As is evident from the microPET images, [^{11}C]HD-800 penetrated the BBB followed by a homogeneous distribution in mouse brain. Blocking with unlabeled HD-800 (5 mg/kg/i.v) 20 min prior to radioligand administration (n = 3) indicates specific binding of radiotracer to brain MTs (Figure 3). The

DOI: 10.1021/acsmedchemlett.8b00060
ACS Med. Chem. Lett. 2018, 9, 452−456

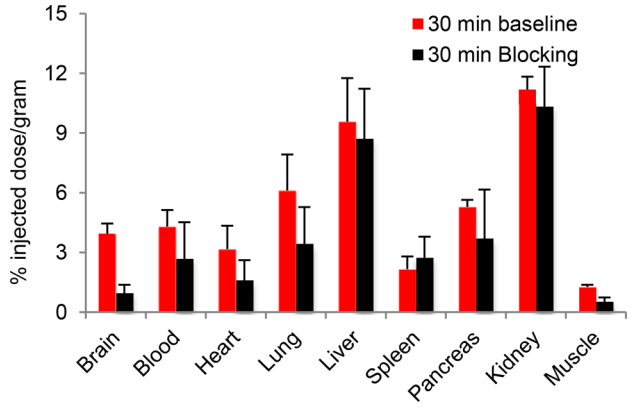

Figure 2. Baseline and blocking biodistribution of [^{11}C]HD-800 in male white mice at 30 min (n = 4). Values are reported as the mean ± SD from four independent experiments.

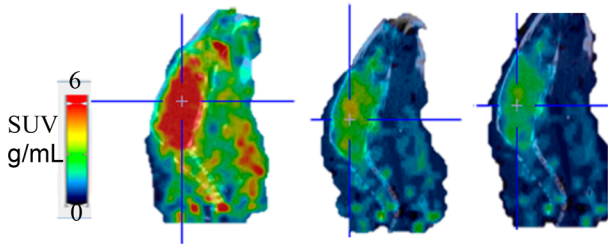

Figure 3. Sum of 0–60 min PET/CT fused sagittal images of [^{11}C]HD-800 in a representative mouse brain (left: baseline; middle: blocking with 5 mg/kg HD-800; right: blocking with 5 mg/kg MPC-6827. Cross lines represent center of brain).

specificity of [^{11}C]HD-800 was further examined by the blocking experiments with a selective colchicine site MT inhibitor MPC-6827 (5 mg/kg/i.v., n = 2, Figure 3).[28] Both blocking agents show significant decreasing activity of [^{11}C]HD-800 in brain. Time activity curves (TACs) further confirm the washout of [^{11}C]HD-800 in mice brain and excellent specific binding with unlabeled HD-800 and MPC-6827 as blocking agents (Figure 4). Blocking with MPC-6827 shows relatively higher specific binding than self-blocking with HD-800. Lack of a suitable reference region is likely to be due

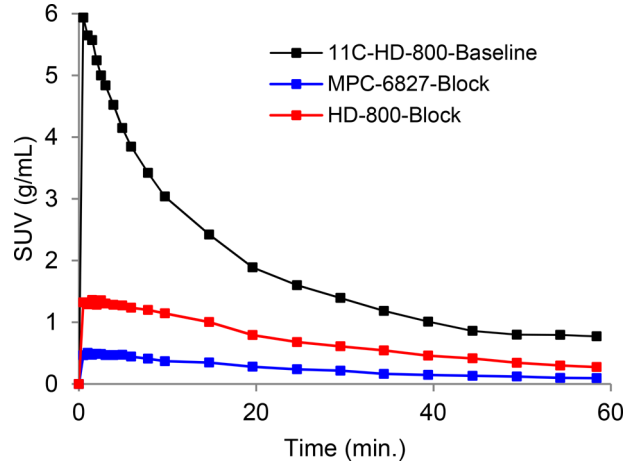

Figure 4. TACs of [^{11}C]HD-800 radioactivity distribution in a representative mouse whole brain.

to ubiquitous distribution of MT in brain but may also be a specific property of this ligand.

In summary, we report a facile synthesis of HD-800 and its radiolabeling precursor and demonstrated an automated radiolabeling procedure for [^{11}C]HD-800 with high RCY, purity, and molar activity. *In vivo* studies in mice indicated BBB penetration, and blocking studies show robust specific binding of the radiotracer in brain and moderate to other organs. [^{11}C]HD-800 did not exhibit interactions with efflux transporters and high brain uptake at the colchicine binding site of MTs in mice. Combination of favorable kinetics and robust specific binding make [^{11}C]HD-800 a suitable PET ligand to be further evaluated for the in vivo quantification of MTs inside and outside the brain. Further evaluation of [^{11}C]HD-800 in nonhuman primates to determine tracer kinetic modeling and feasibility of MT imaging in animals models are underway.

EXPERIMENTAL PROCEDURE

The commercially available chemicals used in the synthesis were purchased from Sigma-Aldrich Chemical Co., (St. Louis, MO), Fisher Scientific Inc. (Springfield, NJ), or other vendors in >95% purity and were used without further purification. ^{1}H NMR spectra were recorded on a Bruker PPX 400-MHz spectrometer. Spectra were recorded in CD_3OD, and chemical shifts (δ) are reported in parts per million (ppm) relative to tetramethylsilane. The mass spectra were recorded on a JKS-HX 11UHF/HX110 HF tandem mass spectrometer in the fast atom bombardment (EI+) mode. Thin-layer chromatography (TLC) was performed using silica gel 60 F254 plates from E. Merck (Aston, PA). High-performance liquid chromatography (HPLC) analyses were performed using a Waters 1525 HPLC system (Milford, MA), and flash column chromatography was performed on silica gel (Fisher 200–400 mesh) using the solvent system indicated in the experimental procedure for each compound. [^{11}C]CO_2 was produced in the Wake Forest PET Center Cyclotron Facility with a GE-PETtrace-800 cyclotron. GE-FX2MeI converts [^{11}C]CO_2 to [^{11}C]CH_4 using a nickel catalyst [shimalite-Ni (reduced)] at 360 °C. [^{11}C]CH_4 was then reacted with gaseous iodine at 760 °C to form [^{11}C]MeI. The purities (chemical and radiochemical) and stability of [^{11}C]HD-800 were determined by reverse phase HPLC (RP-HPLC) (Torrance, CA) with photodiode array and sodium iodide detectors. All animal experiments were conducted under the IACUC approved protocols in compliance with the guidelines for the care and use of research animals established by Wake Forest School of Animal Studies Committee. Biodistribution studies were performed in male white mice, and radioactivity counts were measured using a Wallac 1480 Wizard Gamma Counter, PerkinElmer, Turku, Finland. microPET studies were performed in athymic male nude mice Trifoil PET/CT scanner under anesthetic condition.

HD-800 (**3**): To a solution of 4-chloro-5-methylfuro[2,3-*d*]-pyrimidine (**1**, 85 mg, 0.5 mmol) and 4-methoxy-*N*-methylaniline (**2**, 70 mg, 0.515 mmol) in 3 mL of isopropanol was added 100 μL of *N*,*N*-diisopropylethylamine. The resulting mixture was refluxed at 80 °C for overnight. The reaction mixture was cooled to room temperature, evaporated under high vacuum to remove volatiles and chromatographed over silica gel (5% MeOH-dichloromethane) to afford compound **3** (105 mg, 77%) as brown solid. Analytical data of compound **3** is identical with the product obtained using the previous method.[29]

Desmethyl-HD-800 (**4**): 2 mL anhydrous dichloromethane was added to an argon charged reaction vessel containing HD-800 (81 mg, 0.3 mmol) at 0 °C. 1 M solution of BBr_3 in dichloromethane (1 mL) was added dropwise to the above solution at 0 °C. The solution was stirred for 1 h at room temperature. An aliquot of the reaction mixture was quenched with methanol, analytical HPLC was performed, and complete conversion of HD-800 was confirmed. Subsequently, the reaction was quenched by dropwise addition of methanol (1 mL) at 0 °C, diluted with water (5 mL), and extracted with 50 mL of dichloromethane (2 × 25 mL) followed by 50 mL of ethyl acetate (2 ×

DOI: 10.1021/acsmedchemlett.8b00060
ACS Med. Chem. Lett. 2018, 9, 452–456

25 mL). The combined organic extracts were washed with water and brine and dried over anhydrous $MgSO_4$. Solvent was evaporated under reduced pressure, and the residue obtained was washed with ice cold hexane to obtain compound **4** (65 mg, 85%) as a yellow solid. **4**: ^{1}H NMR (400 MHz, CD_3OD) δ: 1.15 (s, 3H, CH_3), 3.7 (s, 3H, CH_3), 6.8 (d, 2H), 7.2 (d, 2H), 7.5 (s, 1H), 8 (s, 1H); HRMS (EI+) calculated for MH+: $C_{14}H_{14}N_3O_2$: 256.1090; Found: 256.1086.

Alternative synthesis of compound **4**: To a solution of 4-chloro-5-methylfuro[2,3-*d*]pyrimidine (**1**, 85 mg, 0.5 mmol) and 4-(methylamino)phenol (**5**, 63 mg, 0.515 mmol) in 3 mL of isopropanol was added 100 μL of diisopropylethylamine. The resulting mixture was refluxed at 80 °C for overnight. The reaction mixture was cooled to room temperature, evaporated under high vacuum to remove volatiles, and chromatographed over silica gel (5% MeOH-dichloromethane) to afford compound **4** (110 mg, 85%) as a brown solid. Analytical data of compound **4** is identical with the product obtained using the previous method.

Radiosynthesis of [^{11}C]HD-800: [^{11}C]MeI from FX2MeI module was bubbled to the reaction vial placed in FX2M module containing the precursor 4 (~0.5−1 mg) in anhydrous DMF (0.6 mL) and 5 N NaOH aqueous solution (10.0 μL) for ~5 min at room temperature. After the complete transfer of radioactivity, the sealed reaction vial was heated at 80 °C for 5 min. The reaction mixture was quenched with HPLC mobile phase (1.0 mL) and injected onto a reverse-phase semipreparative C18 Phenomenex ODS (250 × 10 mm, 10 μ) HPLC column to purify [^{11}C]HD-800. The isocratic HPLC mobile phase solution consisted of 65% acetonitrile, 35% 0.1 M aqueous ammonium formate buffer solution (pH 6.0−6.5) with UV λ @ 254 nm and a flow rate of 7.0 mL/min. The product [^{11}C]HD-800 (Rt = 6.0−7.0 min) was collected and diluted with 70 mL deionized water and passed through C18 Sep Pak cartridge (WAT036800, Waters, Milford, MA) to trap the radioactive product. [^{11}C]HD-800 was then directly eluted from the cartridge with absolute ethanol (1.0 mL) and formulated with saline (10% ethanol in saline) into a sterile vial through a sterile 0.22 μm pyrogen-free filter for further animal studies and quality control analysis. The chemical and radiochemical purity of [^{11}C]HD-800 aliquot was checked by performing a HPLC injection on analytical Phenomenex C18 HPLC column (250 × 4.6 mm, 5 μ). The mobile phase was 65% acetonitrile and 35% 0.1 M aqueous ammonium formate buffer (pH 6.5); the UV detection was set at 254 nm with a flow rate of 1.0 mL/min. For single injections, 20 μL of [^{11}C]HD800 sample was injected into the Varian analytical HPLC system. Under these QC HPLC conditions, the single injection of [^{11}C]HD800 had a retention time of 6.0 min. The radioactive peak was further authenticated by performing a coinjection with nonradioactive standard HD800, which displayed a similar retention time.

Biodistribution of [^{11}C]HD-800 in mice: Biodistribution experiments were performed male white mice (n = 4, 25 ± 2.5 g). Mice were placed in an induction chamber containing ~2% isoflurane/oxygen and then secured to a custom bed for placement of tail vein catheters. HPLC purified sterile [^{11}C]HD-800 (3.7 ± 0.74 MBq, molar activity 66.5 ± 11.1 GBq/μmol in ~100 μL saline containing 10% ethanol) was administered through tail vein injection. Mice were sacrificed under anesthesia (2% isoflurane) by decapitation via cervical dislocation at 5, 30, and 60 min (n = 4 for each time point). The organs of interest including brain, heart, liver, spleen, lungs, kidney, pancreas, muscle, and blood were removed, weighed, and counted in an automatic γ-counter (Wallac2480 Wizard). Uptake of the radiotracer in different organs and blood was calculated as percentages of injected dose per gram of tissue (%ID/g tissue). Tracer uptakes in the tissues were measured using a γ-counter and expressed in %ID/g tissue. Specific binding was demonstrated by performing blocking studies with unlabeled ligand HD-800 (5 mg/kg, i.v., 100 μL 10% DMSO in water), 20 min prior to radiotracer administration. Dissections were performed at 30 min post radiotracer injection. The blood and organs of interest were isolated and analyzed as described above for the baseline biodistribution study. Parallel to blocking experiment, baseline biodistribution was also performed at 30 min. All experiments were performed in quadruplicate.

MicroPET imaging of [^{11}C]HD-800 in mice: MicroPET imaging experiments were performed in white male mice (n = 3, 25 ± 2.5 g) one by one in the center of the field of view using a Trifoil PET/CT (Triumph II) scanner (1.2 mm resolution and 14 cm axial field of view). Mice were placed in an induction chamber containing ~2% isoflurane/oxygen then secured to a custom double bed for placement of tail vein catheters; anesthesia was maintained via nose-cone at ~1% isoflurane/oxygen for the dynamic imaging procedure. The acquisition started with a CT image acquisition for ~5 min, followed by the intravenous injection of [^{11}C]HD-800 (3.7 ± 0.74 MBq, molar activity 66.5 ± 11.1 GBq/μmol in ~100 μL saline containing 10% ethanol). The total duration of the scan was 60 min. The images were reconstructed using TriFoil attenuation correction and Fourier rebinning in three dimensions in a series of 21 sequential frames of increasing duration from 30 s to 5 min. The CT and PET images were automatically coregistered for analysis. The dynamic images were reconstructed using the TriFoil filtered back-projection 3D-OSEM algorithm with 1 mm voxel size (microPET Manager). The time-activity curves were expressed in g/mL normalized to the injected dose corrected for weight, to obtain standardized uptake values (SUVs). Three mice were used for baseline experiments. For blocking experiments, mice received 5 mg/kg/i.v/100 μL 10% DMSO in water of the unlabeled HD-800 (n = 3) and MPC-6827 (n = 2) 20 min prior to the injection of radiotracer.

■ ASSOCIATED CONTENT

Supporting Information

The Supporting Information is available free of charge on the ACS Publications website at DOI: 10.1021/acsmedchemlett.8b00060.

Molecular formula strings of key chemicals, ^{1}H NMR spectra of compound **4**, binding affinity of HD-800 to brain targets (Table 1), semipreparative HPLC chromatogram of [^{11}C]HD-800, analytical HPLC chromatogram of [^{11}C]HD-800, and analytical HPLC chromatograms of [11C]HD-800 and unlabeled HD-800 (PDF)

■ AUTHOR INFORMATION

Corresponding Author

* Fax: 646-774-7521; Tel: 646-774-7522; E-mail: kmardi@nyspi.columbia.edu.

Author Contributions

$^{\perp}$K.K.S.S. and J.S.D.K contributed equally.

Funding

This work was supported by Diane Goldberg Foundation (CUMC/NYSPI) and Translational Imaging Program (TIP) of the Wake Forest CTSA(UL1TR001420).

Notes

The authors declare no competing financial interest.

■ ACKNOWLEDGMENTS

We thank NIMH-PDSP for competitive binding assay of HD-800.

■ ABBREVIATIONS

AD, Alzheimer's disease; ALS, amyotrophic lateral sclerosis; BBB, blood brain barrier; BPD, bipolar disorder; BCRP, breast cancer resistance protein; CNS, central nervous system; CBD, corticobasal degeneration; CTE, chronic traumatic encephalopathy; DIEA, *N*,*N*-diisopropylethylamine; EOS, end of synthesis; GBM, glioblastoma multiform; HPLC, high-performance liquid chromatography; HSP, hereditary spastic paraplegia; HD, Huntington's disease; MD, major depressive disorder; MAP, microtubule associated protein; MT, micro-

DOI: 10.1021/acsmedchemlett.8b00060
ACS Med. Chem. Lett. 2018, 9, 452−456

tubule; MTA, microtubule targeting agent; MDR1, multidrug resistance protein 1; MS, multiple sclerosis; PD, Parkinson's disease; P-gp, permeability glycoprotein; PET, positron emission tomography; PSP, progressive supranuclear palsy; RCY, radiochemical yield; SCI, spinal cord injury; TAC, time activity curves; TBI, traumatic brain injury; TGI, tumor growth inhibition

REFERENCES

(1) Janke, C. The tubulin code: molecular components, readout mechanisms, and functions. *J. Cell Biol.* **2014**, *206* (4), 461−472.

(2) Barlan, K.; Gelfand, V. I. Microtubule-Based Transport and the Distribution, Tethering, and Organization of Organelles. *Cold Spring Harbor Perspect. Biol.* **2017**, *9* (5), a025817.

(3) Forth, S.; Kapoor, T. M. The mechanics of microtubule networks in cell division. *J. Cell Biol.* **2017**, *216* (6), 1525−1531.

(4) Lockwood, A. H. Molecules in mammalian brain that interact with the colchicine site on tubulin. *Proc. Natl. Acad. Sci. U. S. A.* **1979**, *76* (3), 1184−1188.

(5) Hur, E. M.; Lee, B. D. Microtubule-Targeting Agents Enter the Central Nervous System (CNS): Double-edged Swords for Treating CNS Injury and Disease. *Int. Neurourol. J.* **2014**, *18* (4), 171−178.

(6) Eira, J.; Silva, C. S.; Sousa, M. M.; Liz, M. A. The cytoskeleton as a novel therapeutic target for old neurodegenerative disorders. *Prog. Neurobiol.* **2016**, *141*, 61−82.

(7) Brunden, K. R.; Lee, V. M.; Smith, A. B., III; Trojanowski, J. Q.; Ballatore, C. Altered microtubule dynamics in neurodegenerative disease: Therapeutic potential of microtubule-stabilizing drugs. *Neurobiol. Dis.* **2017**, *105*, 328−335.

(8) Li, L.; Yang, X. J. Tubulin acetylation: responsible enzymes, biological functions and human diseases. *Cell. Mol. Life Sci.* **2015**, *72* (22), 4237−4255.

(9) Dubey, J.; Ratnakaran, N.; Koushika, S. P. Neurodegeneration and microtubule dynamics: death by a thousand cuts. *Front. Cell. Neurosci.* **2015**, *9*, 343.

(10) Bordji, K.; Grandval, A.; Cuhna-Alves, L.; Lechapt-Zalcman, E.; Bernaudin, M. Hypoxia-inducible factor-2α (HIF-2α), but not HIF-1α, is essential for hypoxic induction of class III β-tubulin expression in human glioblastoma cells. *FEBS J.* **2014**, *281* (23), 5220−5236.

(11) Katsetos, C. D.; Dráberová, E.; Legido, A.; Dumontet, C.; Dráber, P. Tubulin targets in the pathobiology and therapy of glioblastoma multiforme. I. Class III beta-tubulin. *J. Cell. Physiol.* **2009**, *221* (3), 505−513.

(12) Oehler, C.; Frei, K.; Rushing, E. J.; McSheehy, P. M.; Weber, D.; Allegrini, P. R.; Weniger, D.; Lütolf, U. M.; Knuth, A.; Yonekawa, Y.; Barath, K.; Broggini-Tenzer, A.; Pruschy, M.; Hofer, S. Patupi-lone (epothilone B) for recurrent glioblastoma: clinical outcome and translational analysis of a single-institution phase I/II trial. *Oncology* **2012**, *83* (1), 1−9.

(13) Fitzgerald, D. P.; Emerson, D. L.; Qian, Y.; Anwar, T.; Liewehr, D. J.; Steinberg, S. M.; Silberman, S.; Palmieri, D.; Steeg, P. S. TPI-287, a new taxane family member, reduces the brain metastatic colonization of breast cancer cells. *Mol. Cancer Ther.* **2012**, *11* (9), 1959−1967.

(14) Mitchell, D.; Bergendahl, G.; Ferguson, W.; Roberts, W.; Higgins, T.; Ashikaga, T.; DeSarno, M.; Kaplan, J.; Kraveka, J.; Eslin, D.; Werff, A. V.; Hanna, G. K.; Sholler, G. L. A Phase 1 Trial of TPI 287 as a Single Agent and in Combination With Temozolomide in Patients with Refractory or Recurrent Neuroblastoma or Medulloblastoma. Pediatr. *Blood Cancer* **2016**, *63* (1), 39−46.

(15) Dubey, J.; Ratnakaran, N.; Koushika, S. P. Neurodegeneration and microtubule dynamics: death by a thousand cuts. *Front. Cell. Neurosci.* **2015**, *9*, 343.

(16) Malamut, M.; Wang, J.-S.; Hong, S.; Oleksandr, X.; Amol, S. V.; Sanjay, T. C. K. A randomized, double-blind, placebo-controlled, multiple ascending dose study to evaluate the safety, tolerability and pharmacokinetics of a microtubule stabilizer (BMS-241027) in healthy females. *Alzheimer's Dementia* **2013**, *9* (4), 668−669.

(17) BMS-241027 (epothilone D): ClinicalTrials.gov identifier: NCT01492374; TPI-288:ClinicalTrials.govidentifier: NCT01966666 and CT02133846.

(18) Cardoso, S. M.; Esteves, A. R.; Arduíno, D. M. Mitochondrial metabolic control of microtubule dynamics impairs the autophagic pathway in Parkinson's disease. *Neurodegener. Dis.* **2012**, *10* (1−4), 38−40.

(19) Clark, J. A.; Yeaman, E. J.; Blizzard, C. A.; Chuckowree, J. A.; Dickson, T. C. A Case for Microtubule Vulnerability in Amyo-trophic Lateral Sclerosis: Altered Dynamics During Disease. Front. *Front. Cell. Neurosci.* **2016**, *10*, 204.

(20) Solowska, J. M.; Baas, P. W. Hereditary spastic paraplegia SPG4: what is known and not known about the disease. *Brain* **2015**, *138* (9), 2471−2484.

(21) Mangas, A.; Coveñas, R.; Geffard, M. New drug therapies for multiple sclerosis. *Curr. Opin. Neurol.* **2010**, *23* (3), 287−292.

(22) Fernández-Nogales, M.; Santos-Galindo, M.; Hernández, I. H.; Cabrera, J. R.; Lucas, J. J. Faulty splicing and cytoskeleton abnormalities in Huntington's disease. *Brain Pathol.* **2016**, *26* (6), 772−778.

(23) Fitzpatrick, M. O.; Dewar, D.; Teasdale, G. M.; Graham, D. I. The neuronal cytoskeleton in acute brain injury. *Br. J. Neurosurg* **1998**, *12* (4), 313−317.

(24) Makinde, H. M.; Just, T. B.; Cuda, C. M.; Perlman, H.; Schwulst, S. J. The Role of Microglia in the Etiology and Evolution of Chronic Traumatic Encephalopathy. *Shock* **2017**, *48* (3), 276−283.

(25) He, M.; Ding, Y.; Chu, C.; Tang, J.; Xiao, Q.; Luo, Z. G. Autophagy induction stabilizes microtubules and promotes axon regeneration after spinal cord injury. *Proc. Natl. Acad. Sci. U. S. A.* **2016**, *113* (40), 11324−11329.

(26) Benítez-King, G.; Valdés-Tovar, M.; Trueta, C.; Galván-Arrieta, T.; Argueta, J.; Alarcón, S.; Lora-Castellanos, A.; Solís-Chagoyán, H. The microtubular cytoskeleton of olfactory neurons derived from patients with schizophrenia or with bipolar disorder: Implications for biomarker characterization, neuronal physiology and pharmacological screening. *Mol. Cell. Neurosci.* **2016**, *73*, 84−95.

(27) Tohyama, M.; Miyata, S.; Hattori, T.; Shimizu, S.; Matsuzaki, S. Molecular basis of major psychiatric diseases such as schizophrenia and depression. *Anat. Sci. Int.* **2015**, *90* (3), 137−143.

(28) Kumar, J. S. D.; Solingapuram Sai, K. K.; Prabhakaran, J.; Oufkir, H. R.; Ramanathan, G.; Whitlow, C. T.; Dileep, H.; Mintz, A.; Mann, J. J. Radiosynthesis and In vivo evaluation of [^{11}C]MPC-6827, the first brain penetrant microtubule PET ligand. *J. Med. Chem.* **2018**, *61* (5), 2118−2123.

(29) Devambatla, R. K.; Namjoshi, O. A.; Choudhary, S.; Hamel, E.; Shaffer, C. V.; Rohena, C. C.; Mooberry, S. L.; Gangjee, A. De-sign, Synthesis, and Preclinical Evaluation of 4-Substituted-5-methyl-furo-[2,3-d]pyrimidines as Microtubule Targeting Agents That Are Effective against Multidrug Resistant Cancer Cells. *J. Med. Chem.* **2016**, *59* (12), 5752−5765.

(30) Wilson, A. A.; Jin, L.; Garcia, A.; DaSilva, J. N.; Houle, S. An admonition when measuring the lipophilicity of radiotracers using counting techniques. *Appl. Radiat. Isot.* **2001**, *54* (2), 203−208.

DOI: 10.1021/acsmedchemlett.8b00060
ACS Med. Chem. Lett. 2018, 9, 452−456